

Cutout shape and reinforcement design for composite C-section beams under shear load

S Guo^{a*}, R Morishima^a, X Zhang^a, A Mills^b

^a *Aerospace Engineering Department, School of Engineering, Cranfield University, Bedford, MK43 0AL, UK*

^b *Materials Department, School of Applied Sciences, Cranfield University, Bedford, MK43 0AL, UK*

Abstract: This paper reports a study of the performance of two forms of cutout and various edge reinforcements in a composite C-section beam under static shear load. Firstly, cutout shape effect on stress concentration was studied. This was followed by a comparative study of a range of reinforcement doublers, which were 20 mm wide rings made of a steel alloy or composite laminate, or by a novel fibre tow placement technique. The comparisons are made in terms of the stress and strain reductions at a hot spot at the cutout edge. Good agreement between the numerical and test results has been achieved for different cutout shapes and reinforcements, and this study has demonstrated that the cutout induced stress concentration can be reduced significantly by appropriate cutout shape and edge reinforcements. The stress reduction magnitude is found to be strongly related to the stiffness of the reinforcement rings. The diamond shaped cutout and the fibre tows reinforcement show clear advantages over the widely adapted circular cutout and laminated ring reinforcement. These findings should contribute to future design improvement of composite aircraft structures in similar shape and loading conditions.

Keywords: Cutout, edge reinforcement, composite channel section, C-section beam, fibre tow placement

Nomenclature

| | |
|--------------------------|--|
| E_i | ply modulus in the i -direction |
| G_{ij} | ply shear modulus in the i - j plane |
| ν_{12} | ply Poisson's ratio in the 1 - 2 plane |
| X_t, X_c | tensile/compressive strength in fibre direction |
| Y_t, Y_c | tensile/compressive strength in transverse direction |
| S | shear strength |
| σ_I | maximum principal stress |
| σ_x, σ_y | direct stress in the x or y -axis |
| τ_{xy} | shear stress in the x - y plane |
| ϵ_x, ϵ_y | direct strain in the x or y -axis |
| γ_{xy} | shear strain in the x - y plane |

* Corresponding author. Tel.: +44 1234 754628; Fax: +44 1234 758203. E-mail address: s.guo@cranfield.ac.uk

1. Introduction

Laminated composites are increasingly used in primary aircraft structures, such as the wing and tailplane spars and ribs as they offer higher stiffness and strength to weight ratio compared to their metallic counterparts. These composite panels often require cutouts for access, inspection, electric and fuel lines, and also for reducing the structural weight. Cutouts lead to stress concentration and reduced buckling load capability. Therefore, the effects of cutouts on laminated composite panels have been investigated by many researchers over the last forty years.

The initial studies were mostly focused on the buckling and postbuckling behaviour of composite plates with cutouts. Nemeth published a review in 1996 on the research activities conducted between 1972 and 1993 on the buckling and/or postbuckling behaviour of composite plates with a cutout [1]. The review has covered many influential factors, such as the cutout size, shape, position and orientation, plate aspect and slenderness ratios, loading and boundary conditions; plate orthotropy and anisotropy were also considered. A further study on the postbuckling behaviour was conducted by Bailey and Wood [2], which studied a square panel with circular and square cutouts and focused on the effect of the cutout diameter to panel length ratio (up to 0.65) on the buckling load carrying capability.

Stress concentration arising from the cutouts has also been a major concern. Rezaeepazhand and Jafari [3] studied the effect of cutout geometry, material properties and fibre angles on the stress distribution around a centrally located cutout in composite plates. Whitworth and Mahase [4] calculated the failure stress and stress concentration around a circular cutout using the Lekhnitskii anisotropy elasticity. Ply-by-ply failure stresses were calculated for three laminates and results showed that higher failure stress and maximum stress concentration occurred at the 0 degree ply. Stress concentration factors (SCFs) for isotropic and orthotropic plates with a circular cutout under uniaxial and biaxial tension were determined by Wu and Mu [5]; they showed that the SCFs depend only on the cutout diameter to plate width ratio. Henshaw et al. [6] calculated the stress concentration in a laminate composite panel with multiple cutouts. They found that stress concentration around the original cutout was significantly increased when a second and third cutout were introduced; the location of additional cutouts also had a great influence on the degree of stress concentration.

One way of reducing stress concentration without adding structural weight is to find the optimum cutout shape. Falzon et al. [7] used the Evolutionary Structural Optimisation (ESO) method to optimise cutout shapes in a square composite panel under different types of loading. They found that under shear load, the optimum cutout shape for a quasi-isotropic laminate was a rectangle of aspect ratio 1.86 and orientated 45° to the horizontal axis. For an isotropic panel the optimum cutout shape was a diamond.

When significant reduction of stress concentration or increment of buckling strength is required, cutout reinforcements are often used. Guo [8] has investigated the effectiveness of different types of reinforcements around a circular cutout in terms of the stress concentration

reduction and improvement of critical buckling load of a composite shear panel. The study has shown that the most significant reduction in stress concentration and the best improvement in buckling stability can be obtained by a pair of rings (doublers) attached to each side of the cutout. Eiblmeier and Loughlan [9-10] studied the buckling response of a laminate panel with a circular cutout reinforced by doublers under different loading and boundary conditions. This investigation showed that buckling stability was increased most efficiently with rings up to 15mm wide.

Another approach to increase cutout load capability is to apply the fibre tow steering technique. Jegley et al. [11-12] demonstrated the effectiveness of tow steered panels to reduce the stress concentration around a cutout and improve the overall panel load carrying capability under both compression and shear loading. Lopes et al. [13] conducted a study on the progressive damage behaviour in postbuckling and final structural failure regime of tow-placed composite panels with a central cutout. Panels with fibre tow placement showed up to 56% higher strength than prepreg laminates. Damage initiation and structural final failure were also significantly delayed for panels fabricated by the fibre tow placement technique.

These extensive research activities were, however, all conducted on flat panels and till today few studies have been published on realistic composite beam structures. The effect of cutout shape and the effectiveness of different types of cutout reinforcement in a composite beam are yet to be investigated.

This paper reports a recent investigation into the design of cutout shape and reinforcement for a composite C-section beam subjected to shear load. The objective is to reduce the cutout stress concentration by bonding various edge reinforcements that are made of different materials. The effectiveness of conventional metal reinforcement rings was compared to composite rings made of either prepreg laminate or fibre tows. Finite element analysis and experimental tests were conducted and good agreement has been achieved for different cutout shapes and reinforcements. The novel fibre tow reinforcement shows clear advantage over the conventional rings.

2. The C-section beams

Constant C-section composite beams were designed for FE analysis and experimental tests. Each beam is of 650 mm in length and 200 mm in web depth and 100 mm flange width. Some beams have a single cutout of either circular or diamond shape, and others have double cutouts of one circular and one diamond. Figures 1a and b show the dimensions of the single and double cutout beams. Some cutouts were reinforced around the perimeter by means of rings (doublers) made of either a steel alloy or carbon composite laminate, or the fibre tow placement technique. The geometry of the rings is given in Fig. 1c. The steel rings are 1.5 mm thick and 20 mm wide, the laminate rings are 2 mm thick and 20 mm wide made of 8-ply quasi-isotropic (QI) carbon-epoxy prepreg, and the fibre tow rings are 6-ply carbon fibres of total thickness of 1.5 mm. Strain gauge positions are illustrated in Fig. 1d and e. Strains were

measured at positions marked A, A' and B by mounting strain gauge rosettes each consisting of three gauges in the x , y and 45° directions. For shear loaded panels, stress concentration occurs near point A.

2.1 Manufacturing

To validate the numerical analysis, four beam specimens with different cutout and reinforcement designs were made and tested. These test samples were manufactured by Cranfield University's Department of Materials. The beams were laminated by hand using Hexply UDM21/35%/268/T800S prepreg. To form the 'C' beam sections using an aluminium male tool, each set of four plies was debulked using a vacuum bag so as to minimise corner fibre wrinkling. The beams were consolidated and cured in an autoclave at 6 bar and up to 180°C for a total cure time of 7 hours. An Airtech Airpad rubber intensifier was used as a female tool under the vacuum bag to provide a smooth outer surface. The cutouts in the beam were made using a GFM water jet cutting machine.

The three types of reinforcing rings were produced using two techniques. For the steel and composite laminate, water jet cutting of plate was used. For the fibre tow reinforced ring, a net shape ring was manufactured using a single prepreg tow. This was wound around a mandrel of an outer diameter matching the hole diameter, constrained perpendicular to the mandrel using side plates, then autoclave cured by the same process as for the laminate. The reinforcing rings were bonded at 50°C for four hours using the Huntsman Araldite 420 A/B two component epoxy paste adhesive.

2.2 Materials

All test samples were made of the Hexply M21/T800S carbon-epoxy prepreg that came in a roll of 300 mm wide and ply thickness of 0.25 mm. Samples were fabricated in symmetric layup $[\pm 45/0/\pm 45/90/\pm 45]_s$ to a final thickness of 4 mm (16 plies) for the beam web and flanges. The mechanical properties of the laminate are given in Table 1.

2.3 Cases studied in this work

Table 2 summarises all the study cases with details being described below. All design cases have been modelled by the FEM and some of them are validated by experimental tests. Each cantilever beam was subjected to a 20 kN vertical load applied at its free end and near its shear centre, which is equivalent to a nominal applied shear stress of 23 MPa (average) or 28 MPa (maximum).

Example 1 – single cutout.

Each beam sample contains a cutout of either circular or diamond shape and is clamped at one end and subjected to a vertical load at the other end through the beam section shear centre. Four different scenarios have been studied to include two cutout shapes and two types of edge reinforcement which are: 1.1) un-reinforced diamond cutout; 1.2) un-reinforced circular

cutout; 1.3) circular cutout reinforced by a pair of composite laminate rings made of the same material as the beam and bonded to both sides of the cutout; 1.4) circular cutout reinforced by a pair of carbon fibre tow rings bonded to both sides of the cutout.

Example 2 – double cutouts with the circular cutout near the clamping end.

Beam sample is clamped at the end near the circular cutout and subjected to a vertical load at the other end through the beam section shear centre. Cutout that is nearer to the clamp end is subjected to severer loads, hence attention is focused on the strains and stresses around the circular cutout. Three cases have been studied: 2.1) un-reinforced cutouts; 2.2) both cutouts were reinforced by a pair of laminate rings bonded to both sides of the cutout; 2.3) reinforced circular cutout by a pair of steel rings bonded to both sides of the cutout.

Example 3 – double cutouts with the diamond cutout near the clamping end.

Using the same beam as the example 2 but switching the support ends, attention is now focused on the stresses and strains around the diamond cutout and the interaction effect. Three cases have been studied: 3.1) un-reinforced cutouts; 3.2) reinforced by a pair of laminate rings bonded to both sides of the cutouts; 3.3) reinforced cutouts by a pair of steel rings.

3. Numerical modelling

3.1 Modelling approach

All design cases presented above have been modelled by the finite element method to determine the stress concentration around these cutouts. The commercial FE code MSC PATRAN/NASTRAN was used to create the C-section beam models and to carry out numerical analyses. The flanges and beam web were modelled using quadrilateral linear shell elements (QUAD4) and the IsoMesh facility. The QUAD4 elements are capable of modelling composite properties. The reinforcement rings were also modelled by the shell elements and the offset command was used to separate the surfaces representing the beam web and the ring respectively. Material properties, boundary and loading conditions were implemented in the model using the appropriate tools offered by PATRAN. A typical FE model has 11461 shell elements.

3.2 Numerical results

Single cutout without reinforcement (cases 1.1 and 1.2)

Comparison is made between the un-reinforced diamond and circular cutouts under the same loading ($P = 20$ kN) and boundary conditions. FE stress contour maps are shown in Fig. 2, which indicates that the stress concentration around the diamond cutout is less severe than that of the circular cutout. The maximum principal stress (σ_1) is 155 MPa for the diamond and 167 MPa for the circular cutout.

FE calculated maximum stresses and strains are listed in Table 3. These values are calculated at the maximum stress point for the different cutouts. The FE results indicate that the

maximum stress is at the 130° position for the circular cutout (Fig. 2a) and 100° position for the diamond (Fig. 2b). Table 3 indicates that all the stress and strain components are generally lower around the diamond cutout. In terms of the maximum in-plane shear stains (γ_{xy}), the difference between the diamond and the circular is about 16% (1726 vs. 2049 $\mu\epsilon$). In terms of the maximum x -direction stains (ϵ_x), the difference between the diamond and the circular is about 17% (1760 vs. 2130 $\mu\epsilon$). Therefore, the FE results indicate that the diamond cutout can reduce the stress concentration by about 16-17%.

Single circular cutout with reinforcement rings (cases 1.3 and 1.4)

When the single circular cutout are reinforced by a pair of composite rings (cases 1.3 and 1.4), stress concentration reduction is significant in all stress components. Table 4 shows the calculated average stress and strain components at the measurement point A (Fig. 1c). The reduction in the principal stress (σ_I) is 31% (unreinforced web stress 113 MPa versus the reinforced web stress of 78 MPa) when using the laminate reinforcement rings (cases 1.3), and stress reduction becomes much higher at 43% (113 MPa vs. 64 MPa) when the fibre tow rings are employed (cases 1.4).

These reinforcement rings work like doublers that are designed to pick up loads and relieve the stresses around the cutout on the beam web. Since the strain values are the same on the beam web and the attached rings, the laminate rings that have the same elastic modulus as the web laminate will bear the same average stress as the material around the cutout edge on the web. This is demonstrated by the FE calculated principal stresses in the laminate ring and the web, i.e. $\sigma_{I_ring} = 76$ MPa and $\sigma_{I_web} = 78$ MPa from Table 4 case 1.3. The numerical results also show that the fibre tow rings can pick up more stresses from the web, e.g. $\sigma_{I_ring} = 129$ MPa versus $\sigma_{I_web} = 64$ MPa from Table 4 case 1.4. This difference in stress transfer capability can be explained by the difference in the elastic modulus of the fibre tows and that of the quasi-isotropic laminate ring.

To quantify the load transfer capability, stiffness ratio of two different rings is defined as:

$$r = \frac{E_{1a}t_a}{E_{1b}t_b} \quad (1)$$

where t_a and t_b are the thickness, and E_{1a} and E_{1b} the equivalent elastic constant (modulus) of the two different reinforcement rings, respectively. Subscript “1” indicates the modulus in a specific direction.

Assign E_{1b} as the modulus of the quasi-isotropic laminate ring (case 1.3) that is calculated as 64.7 GPa by the laminate theory, and E_{1a} as the fibre tow modulus (case 1.4) that has a range of values depending on the position of fibre tows winding around the cutout perimeter. Since the strain gauge rosette covers an area of 4 x 4 mm (gauge length), the measurement point represents an arc length that subtends an angle of 5.7 degree along the circumference. The upper bound value of E_{1a} is estimated as 172 GPa when the fibre tow is at the centre of the

measurement point A and the fibres are exactly in 45° direction; the lower bound value is estimated as 130 GPa when the fibre tow is displaced from the measurement centre by ±2.85 degree. The thickness of the fibre tow ring t_a is 1.5 mm and the laminate ring t_b is 2 mm. According to eq. (1), the stiffness ratio of the two rings is between 1.52 (lower bound) and 1.99 (upper bound), resulting in an average stiffness ratio of 1.75, which is very close the ratio of the stresses transferred to the two rings that is 1.70 (based on calculated $\sigma_{I_tow_ring} = 129$ MPa & $\sigma_{I_lam_ring} = 76$ MPa in Table 4). Hence considerably higher load transfer capability is achieved by the fibre tow ring owing to its better performance in the fibre direction.

For each case, stresses in each laminate ply in the beam web as well as in the rings were calculated. An example is presented in Fig 3, which shows the principal stress in each ply when the circular cutout is reinforced by a pair of the laminate rings (case 1.3) or fibre tow rings (case 1.4), and both cases are compared with the un-reinforced cutout (case 1.2). These stress values correspond to a particular calculation point within the strain gauge covered area that is marked as point A in Fig.1; they are not the average stress values over the strain gauge region. Fig 3(a) shows the principal stress in the beam web around the cutout. In terms of the stress relief around the cutout, the fibre tow ring reduces more stress in the 45° ply, whereas it is less effective in reducing the 0° ply stress comparing to the laminate ring case. Fig. 3(b) shows the principal stress in the laminate ring and fibre tow ring. The laminated ring picks up more stress by the 0° and 45° plies, but it is less effective in the -45° and 90° plies.

Double cutouts with the circular cutout near the clamping end (cases 2.1, 2.2 & 2.3)

Cases in example 2 were studied under the same load ($P = 20$ kN) and support conditions. Figure 4 shows an FE calculated contour of the principal stress for the unreinforced cutouts (case 2.1). Although there is little interaction effect of the two cutouts, the stress concentration at the circular cutout is more severe than that of singular cutout (case 1.2 Fig. 2a) due to the additional diamond cutout. The hot spot is still at point A where strain gauges were mounted. The maximum principal stress is 193 MPa, whereas for the single circular cutout the maximum principal stress is 167 MPa

A summary of FE stress and strain results is presented in Table 5. When the cutouts are reinforced by a pair of laminated composite rings (case 2.2) or steel rings (case 2.3), stress concentration reduction is significant in all stress components. In terms of the principal stress (σ_j), the reduction of the maximum stress is 42% when the laminated rings are bonded ($\sigma_{I_unreinforced} = 138$ MPa vs. $\sigma_{I_laminated_ring} = 79$ MPa), and the reduction is increased to 49% when using the steel rings (138 MPa vs. 70 MPa).

These reinforcement rings were bonded and cured at 50°C. Therefore for the steel ring case, due to the mismatch of the coefficients of thermal expansion, some thermal residual stresses will be present on the rings and the web at the room temperature (25°C). However, the temperature difference of 25°C is small and the strain gauges were mounted after the curing process in room temperature and the strain data acquisition device was set to zero at the

beginning of the test. Therefore, residual stresses arising from the bonding process at elevated temperature are not taken into account in this work.

In the absence of the thermal residual stresses, the stiffness of the rings influences the load transfer capability between the beam web and the reinforcement rings. According to eq. (1) and assigning E_{1a} and E_{1b} with the elastic modulus of the steel (193 MPa) and quasi-isotropic laminate (64.7 MPa), t_a and t_b the thickness of the steel (1.5 mm) and laminate rings (2 mm), respectively, the stiffness ratio of the two rings is 2.24.

In terms of the FE calculated principal stress (Table 5), the stresses picked up by the steel and laminate rings are 177 MPa and 77 MPa, respectively. These give a stress ratio of 2.30, which is very close to the stiffness ratio of 2.24. Therefore it can be said that in the absence of the curing residual stresses the stress transfer capability is mainly governed by the stiffness of the doubler rings. In this case the steel rings are much more effective than the composite laminate rings even though they are 25% thinner at 1.5 mm comparing to the 2 mm thick laminate rings. However, the steel rings are much heavier than that of the composite laminate rings. In this case the weight of the steel ring is 0.26 kg (based on steel density of 8000 kg/m³) whereas the weight of the laminate ring is only 0.08 kg (based on laminate density of 1580 kg/m³) – a factor of 3.25. A trade off between the load carrying capability and structural weight is important in a balanced design.

Figure 5 presents the principal stress in each ply when the circular cutout is reinforced by a pair of laminate rings (case 2.2) or steel rings (case 2.3) and a comparison with the unreinforced cutout (case 2.1). The stress values presented in Fig. 5 correspond to a particular FE model point within the strain gauge covered area that is marked as point A in Fig. 1. Firstly, Fig 5(a) shows that stresses are lower in the reinforced beam web in all plies. In terms of the stress relief in the beam web around the cutout, the steel rings are more effective than the laminate rings due to its much higher stiffness (stiffness ratio of the two rings is 2.24). The steel rings are also effective for all laminate orientations due to its isotropic properties. This contrasts to the fibre tow rings (case 1.4), which works well only in the local fibre direction. Fig. 5(b) shows the principal stress in the laminate rings and steel rings. The laminate rings pick up more stress by the 0° and 45° plies, but the -45° and 90° plies are less effective. The average stress in the steel ring is about 156 MPa, whereas the average stress over the eight-ply laminate ring is about 75 MPa – giving a ratio of 2.1 for stress transfer capability.

Double cutouts with the diamond cutout near the clamping end (cases 3.2 & 3.3)

For the study cases in example 3 under the same loading ($P=20$ kN) and support conditions, a summary of FE strain and stress results is presented in Table 6.

As example 2, the stress concentration reduction is significant in all stress components when the cutouts are reinforced by a pair of laminated composite rings (cases 3.2) or steel rings (case 3.3) as summarised in Table 6. In terms of the principal stress (σ_1), the reduction of the

maximum local stress is 27% (94 MPa vs. 69 MPa) if using the laminated rings, and the reduction is increased to 41% (94 MPa vs. 55 MPa) when using the steel rings. The magnitude of stress reduction is also significant as in cases 2.2 and 2.3. The same comments hold for the predominant effect of the ring material stiffness as discussed for Example 2.

4. Validation and discussions

Four beam samples with different cutout and reinforcement designs were manufactured and tested. These were the samples for case 1.2, 1.4, 2.2 and 2.3 (Table 2). Photographs in Fig. 6 show beam samples mounted in the test rig for the study case 1.4 and 2.2. Strains were measured at points A and B by mounting strain gauge rosettes each consisting three gauges in the x , y and 45° directions. Additional strain measurement was performed for case 2.3 at the diamond cutout and this is denoted as case 2.3D in the following result presentations.

Comparisons of the measured and FE calculated strains are given in Table 7. The strains in case 2.3D were measured at point A' as shown in Fig. 1e for the diamond cutout near the load end. Since the strain gauge position A' is on the lower half of the beam specimen, the strain readings reverse the sign. Take the x -axis strain as example which is the most concerned strain component in the beam bending problem. For the single cutout, the relative error in ε_x for case 1.2 is 6% and for case 1.4 is 1.1%. For the double cutouts the relative error for case 2.3D is 6.5% and the worst case is for test 2.3 with error 19.5%. The agreement between the measurements and FE results are fairly good for the x -axis strains. For the y -axis and shear strain components, there are occasional disparity between the FE and the experimental results. However, we do not feel that this is significant.

Figure 7 presents a comparison of the stress components obtained by the tests and FEA. The "test" stresses are calculated by multiplying the measured strain values with the equivalent elastic modulus. The agreement is generally good.

Conclusions

Numerical modelling and experimental tests have been conducted to study the stress concentration around cutout edges in a composite C-section beam under the in-plane shear load. Following conclusions can be drawn.

Without edge reinforcement a diamond-shape cutout reduces stress concentration by about 16% comparing to a circular cutout.

For a circular or diamond cutout, edge reinforcement by bonding a pair of rings made of a steel alloy, carbon composite laminate, or fibre tows, has shown effective stress reduction. In the absence of the thermal residual stresses arising from elevated temperature curing process, the stiffness ratio of the ring to the substrate plays the most important role in quantifying the amount of load transfer from the substrate to the reinforcement rings.

For the same geometries, rings made by the steel alloy provide the most effective stress reduction around cutout edges. Rings fabricated by the fibre tow placement technique rank the

second. However, the weight penalty by the steel rings is three times more than that of carbon fibre rings, whereas the magnitude of stress reduction offered by the steel ring is about 1.24 times of that by the fibre tow rings.

Acknowledgements

The authors are grateful to Caden Stiles for his contribution to some of the experimental tests.

References

1. Nemeth MP. Buckling and postbuckling behaviour of laminated composite plates with a cutout, NASA Technical Paper 3587, 1996.
2. Bailey R, Wood J. Stability characteristics of composite panels with various cutout geometries, *Composite Structures*, 1996; 35: 21-31.
3. Rezaeepazhand J, Jafari M. Stress analysis of perforated composite plates, *Composite Structures*, 2005; 71: 463-468.
4. Whitworth HA, Mahase H. Failure of orthotropic plates containing a circular opening, *Composite Structures* 1999; 46: 53-57.
5. Wu H-C, Mu B. On stress concentrations for isotropic/orthotropic plates and cylinders with a circular hole, *Composites Part B: Engineering* 2003; 34: 127-134.
6. Henshaw JM, Sorem JR, Glaessgen Jr EH. Finite element analysis of ply-by-ply and equivalent stress concentrations in composite plates with multiple holes under tensile and shear loading, *Composite Structures* 1996; 36: 45-58.
7. Falzon BG, Steven GP, Xie YM. Shape optimization of interior cutouts in composite panels, *Structural and Multidisciplinary Optimization* 1996; 11: 43-49.
8. Guo S. Stress concentration and buckling behaviour of shear loaded composite panels with reinforced cutouts, *Composite Structures* 2007; 80: 1-9.
9. Eiblmeier J, Loughlan J. The buckling response of carbon fibre composite panels with reinforced cut-outs, *Compos. Struct.* 1995; 32: 97-113.
10. Eiblmeier J, Loughlan J. The influence of reinforcement ring width on the buckling response of carbon fibre composite panels with circular cut-outs, *Composite Structures* 1997; 38: 609-622.
11. Jegley D, Tatting B, Adoptech, Gürdal Z. Optimization of elastically tailored tow-placed plates with holes, 44th AIAA/ASME/ASCE/AHS/ASC Structures, Structural Dynamics, and Materials Conference, Norfolk, Virginia, 7-10 Apr 2003. AIAA-2003-1420.
12. Jegley D, Tatting B, Gürdal Z. Tow-steered panels with holes subjected to compression or shear loading, 46th AIAA/ASME/ASCE/AHS/ASC Structures, Structural Dynamics and Materials Conference. Austin, TX, April 2005; AIAA-2005-2017.
13. Lopes CS, Camanho PP, Gürdal Z, Tatting BF. Progressive failure analysis of tow-placed, variable-stiffness composite panels, *Int J Solids & Structures*, In Press, Available online 6 July 2007.

Table 1 Mechanical properties of M21/T800S prepreg *

| Material | E_1 (GPa) | E_2 (GPa) | G_{12} (GPa) | ν_{12} | X_t (MPa) | X_c (MPa) | Y_t (MPa) | Y_c (MPa) | S (MPa) | ρ (Kg/m ³) |
|----------|----------------|----------------|-------------------|------------|----------------|----------------|----------------|----------------|--------------|--------------------------------|
| M21 | 172 | 10 | 5 | 0.3 | 3939 | 1669 | 50 | 250 | 79 | 1580 |

* Data source: <http://www.hexcel.com/products/matrix%20products/prepregs>, accessed 4 Sept 2007.

Table 2 Summary of study cases reported in this paper.

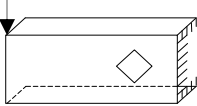
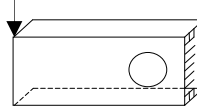
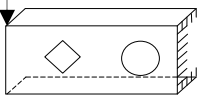
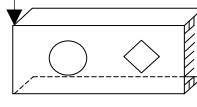
| Case | Description | Study Method |
|------|---|--------------|
| 1.1 | Single diamond cutout, no reinforcement  | FEA |
| 1.2 | Single circular cutout, no reinforcement  | FEA, Test |
| 1.3 | Single circular cutout, with laminate reinforcement rings | FEA |
| 1.4 | Single circular cutout, with fibre tow reinforcement rings | FEA, Test |
| 2.1 | Double cutouts, no reinforcement  | FEA |
| 2.2 | Double cutouts, with laminate reinforcement rings | FEA, Test |
| 2.3 | Double cutouts, with steel reinforcement rings | FEA, Test |
| 3.1 | Double cutouts, no reinforcement  | FEA |
| 3.2 | Double cutouts, with laminate reinforcement rings | FEA |
| 3.3 | Double cutouts, with steel reinforcement rings | FEA |

Table 3 Calculated maximum stresses and strains around unreinforced diamond and circular cutout in Example 1 (stress unit: MPa; strain unit: $\mu\epsilon$)

| Case | ϵ_x | ϵ_y | γ_{xy} | σ_x | σ_y | τ_{xy} | σ_l |
|------|--------------|--------------|---------------|------------|------------|-------------|------------|
| 1.1 | 1760 | 847 | 1726 | 106 | 68 | 59 | 155 |
| 1.2 | 2130 | 1520 | 2049 | 112 | 90 | 70 | 167 |

Note: σ_l is the principal stress obtained directly from the FE analysis.

Table 4 Calculated average stresses and strains at point A of Example 1 (units: MPa, $\mu\epsilon$).

| Case | ϵ_x | ϵ_y | γ_{xy} | σ_x | σ_y | τ_{xy} | σ_l | Weight (Kg) |
|------|--------------|--------------|---------------|-----------------------|-----------------------|-----------------------|------------------------|-------------|
| 1.1 | 733 | 183 | 1182 | 51 | 35 | 41 | 92 | 1.57 |
| 1.2 | 1054 | 157 | 1258 | 70 | 43 | 43 | 113 | 1.79 |
| 1.3 | 642 | 164 | 960 | 45 (web) 50 (ring) | 31 (web) 26 (ring) | 33 (web) 24 (ring) | 78 (web) 76 (ring) | 1.83 |
| 1.4 | 700 | 45 | 494 | 45 (web) 59 (ring) | 22 (web) 50 (ring) | 17 (web) 51 (ring) | 64 (web) 129 (ring) | 1.82 |

Table 5 Calculated average stresses and strains at point A for Example 2 (units: MPa, $\mu\epsilon$).

| Case | ϵ_x | ϵ_y | γ_{xy} | σ_x | σ_y | τ_{xy} | σ_l | Weight (Kg) |
|------|--------------|--------------|---------------|------------------------|-----------------------|-----------------------|------------------------|-------------|
| 2.1 | 1126 | 323 | 1634 | 80 | 56 | 56 | 138 | 1.54 |
| 2.2 | 643 | 167 | 964 | 45 (web) 50 (ring) | 32 (web) 27 (ring) | 33 (web) 24 (ring) | 79 (web) 77 (ring) | 1.62 |
| 2.3 | 517 | 184 | 892 | 38 (web) 129 (ring) | 28 (web) 76 (ring) | 31 (web) 70 (ring) | 70 (web) 177 (ring) | 1.8 |

Table 6 Calculated average stresses and strains at point A for example 3 (units: MPa, $\mu\epsilon$).

| Case | ϵ_x | ϵ_y | γ_{xy} | σ_x | σ_y | τ_{xy} | σ_I |
|------|--------------|--------------|---------------|------------|------------|-------------|------------|
| 3.1 | 791 | 154 | 1245 | 54 | 35 | 41 | 94 |
| 3.2 | 414 | 197 | 986 | 33 (web) | 27 (web) | 33 (web) | 69 (web) |
| | | | | 34 (ring) | 23 (ring) | 24 (ring) | 63 (ring) |
| 3.3 | 321 | 162 | 398 | 26 (web) | 22 (web) | 27 (web) | 55 (web) |
| | | | | 82 (ring) | 58 (ring) | 62 (ring) | 134 (ring) |

Table 7 Comparison of measured and calculated strains at point A & A' (unit: $\mu\epsilon$).

| Cases | Measurement | | | FEA | | |
|-------|--------------|--------------|---------------|--------------|--------------|---------------|
| | ϵ_x | ϵ_y | γ_{xy} | ϵ_x | ϵ_y | γ_{xy} |
| 1.2 | 991 | 355 | 1589 | 1054 | 157 | 1258 |
| 1.4 | 692 | 93 | 486 | 700 | 45 | 494 |
| 2.2 | 580 | 246 | 1660 | 643 | 167 | 964 |
| 2.3 | 416 | 245 | 1049 | 517 | 184 | 892 |
| 2.3D | -250 | -169 | 597 | -268 | -202 | 745 |

Figures

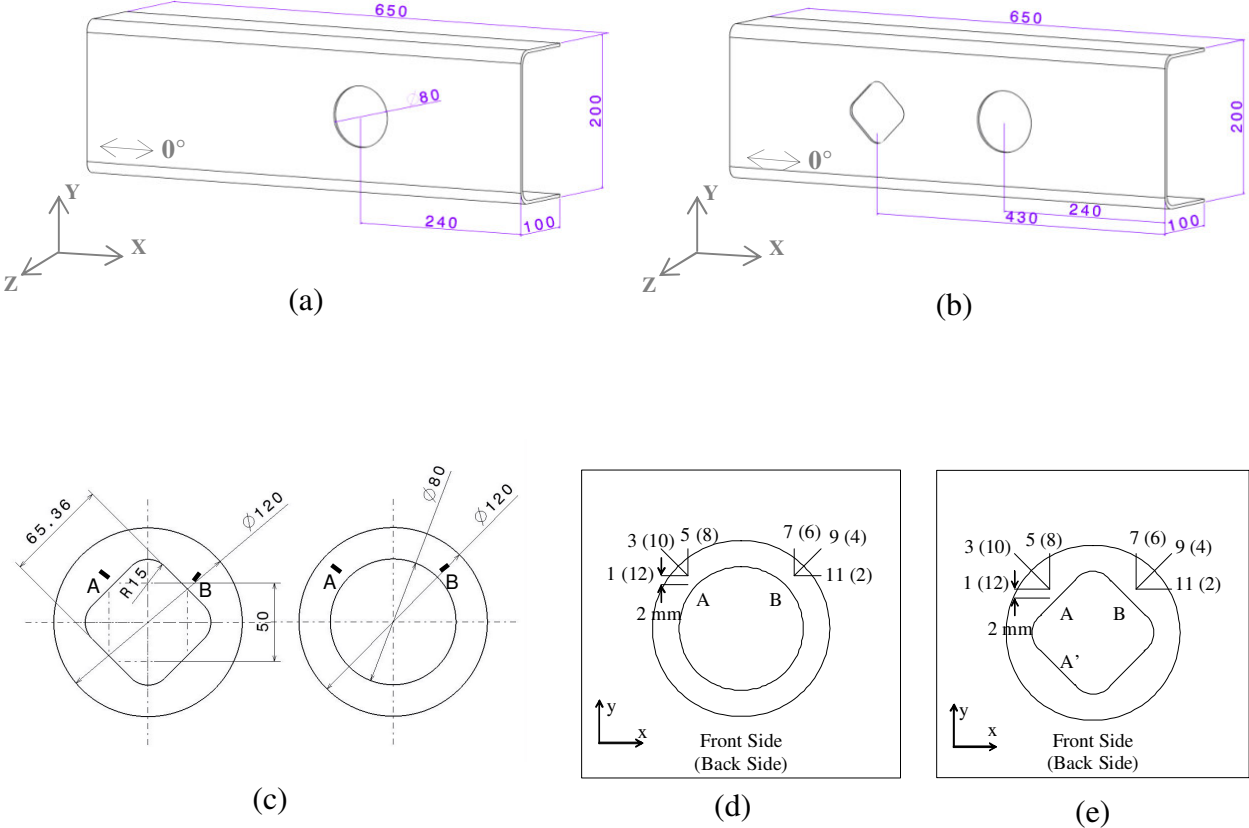
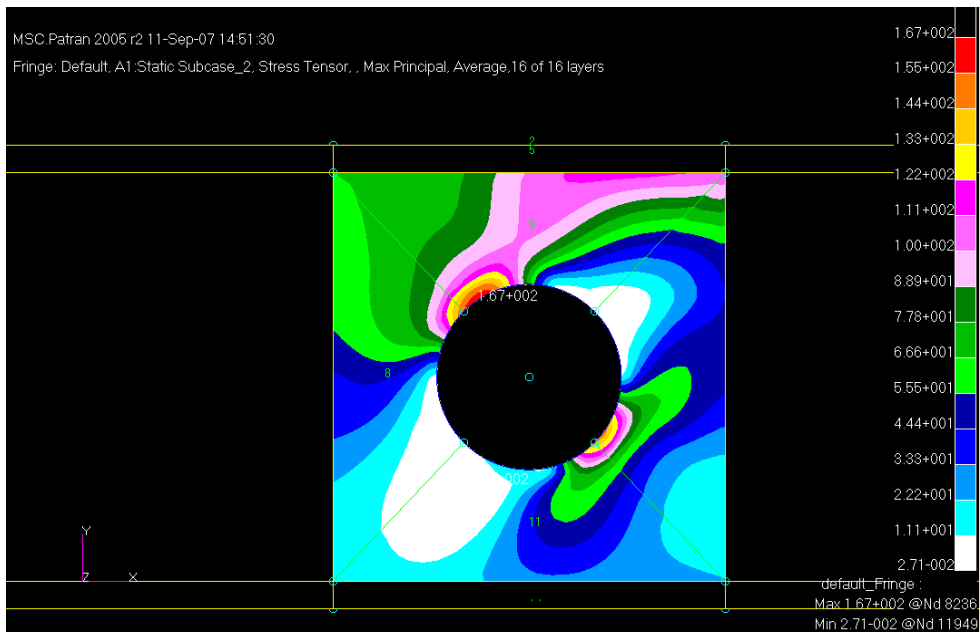
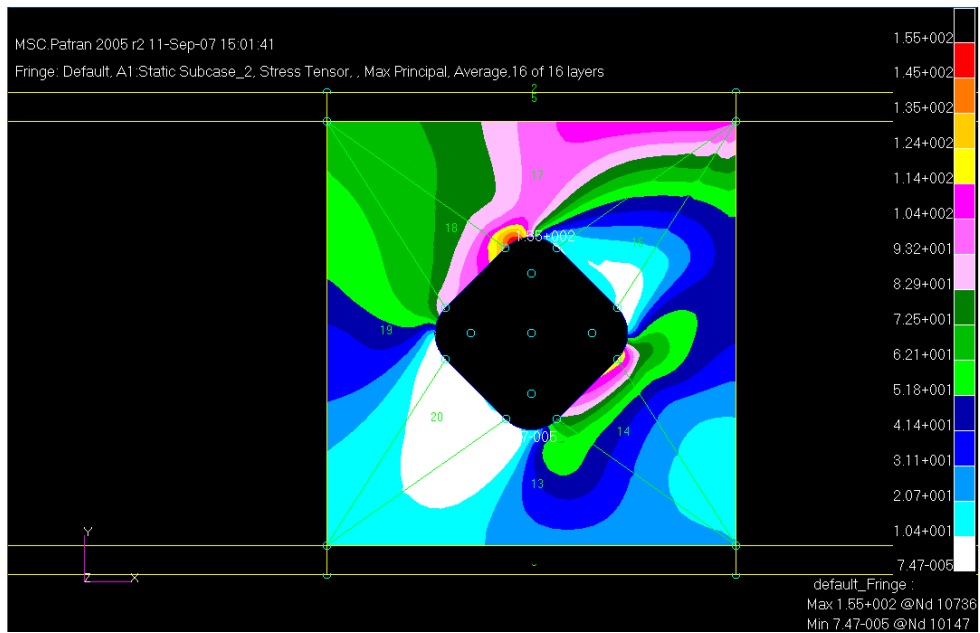


Figure 1 (a) single cutout in a C-section beam; (b) double cutouts in a C-section beam; (c) dimensions of the diamond and circular cutouts and reinforcements; (d) and (e) dimensions and strain gauge positions for the circular and diamond cutout (unit: mm).



(a)



(b)

Figure 2. FE principal stress contours of unreinforced single cutout: (a) case 1.2 circular cutout (maximum stress 167 MPa); (b) case 1.1 diamond cutout (maximum stress 155 MPa).

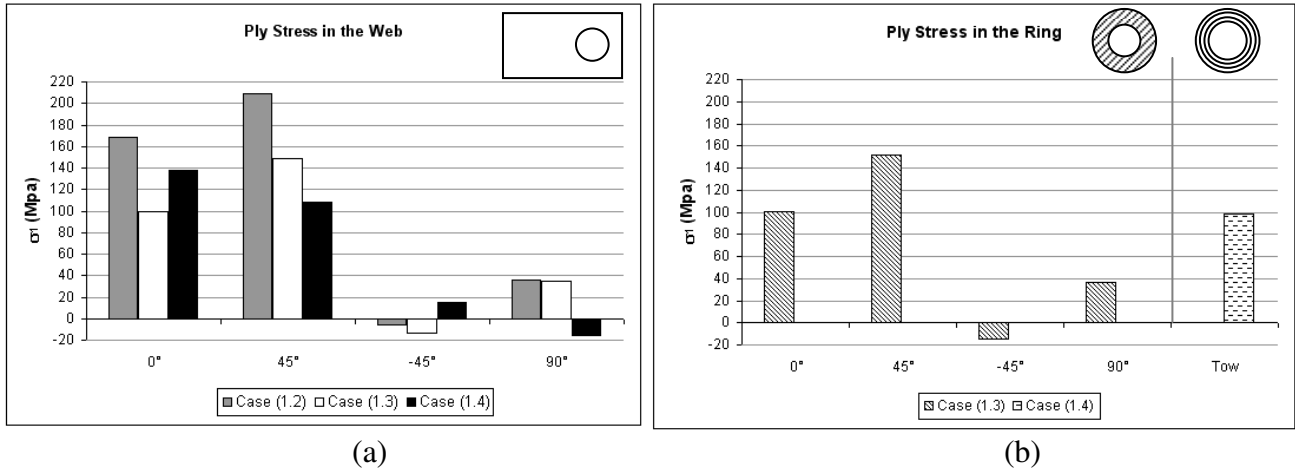


Figure 3. Maximum principal stress in each ply for Example 1: (a) in the beam web around cutout; (b) in the laminate ring and average stress in fibre tow ring. Note: these stresses were computed at a particular point in the FE model within the strain gauge covered area that is defined as point A.

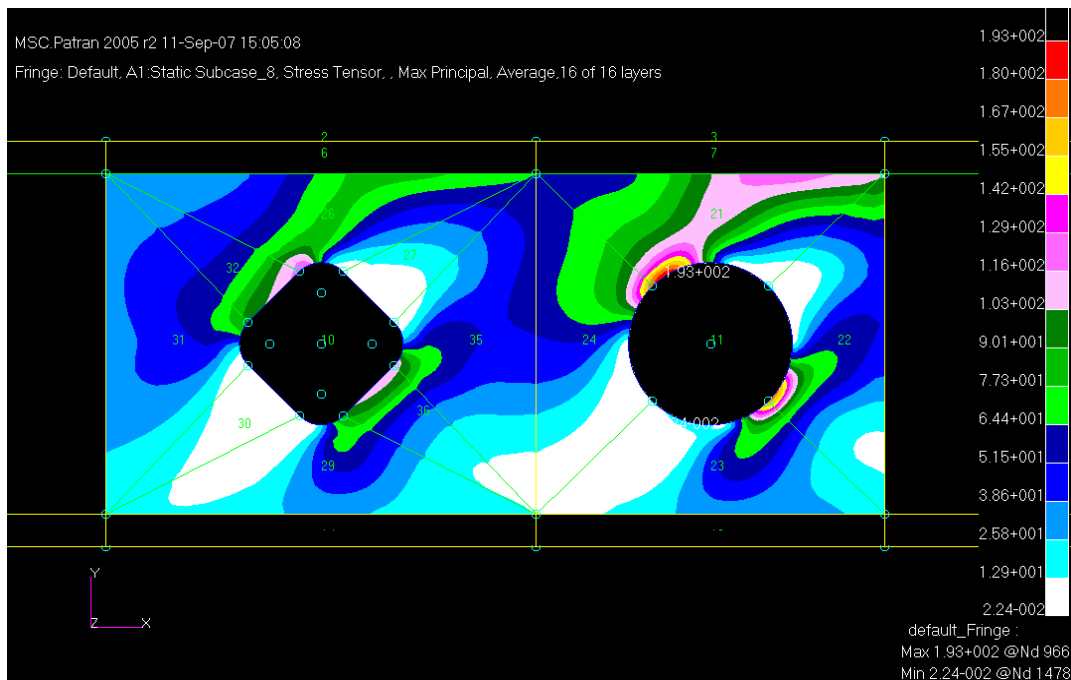
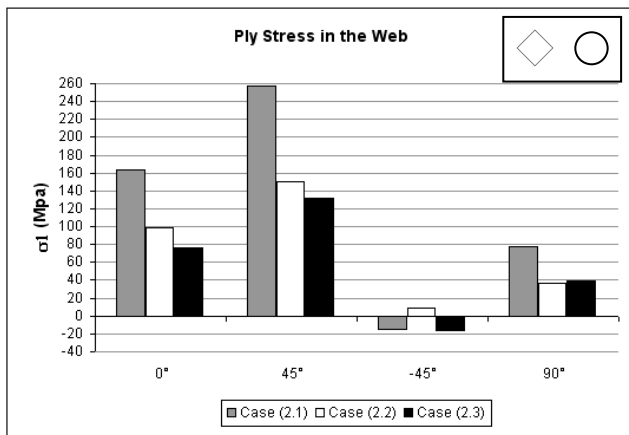
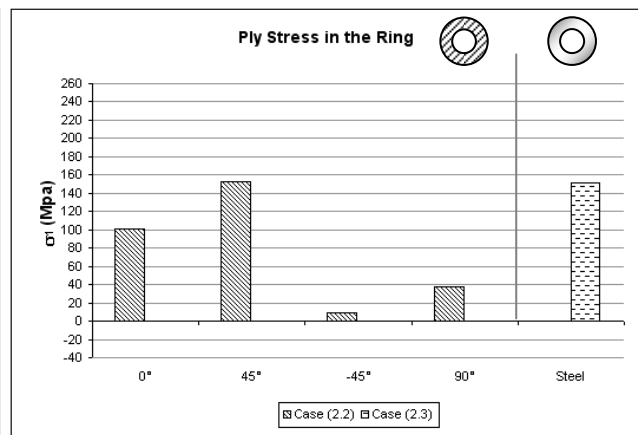


Figure 4. Principal stress contour map of the double cutouts in Example 2 and interaction effect of the two cutouts; maximum stress at circular cutout 193 MPa; maximum stress at diamond cutout 129 MPa.

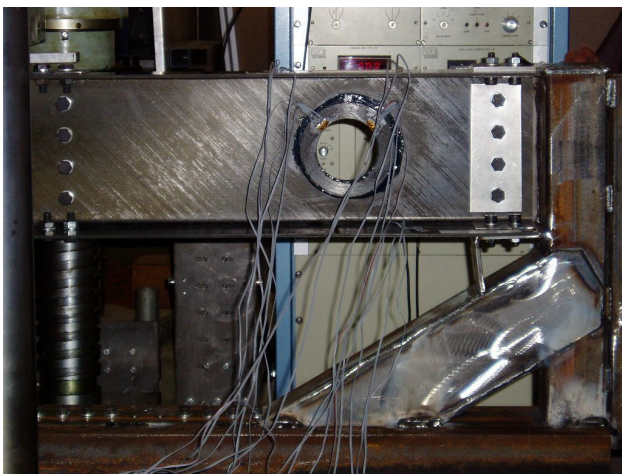


(a)

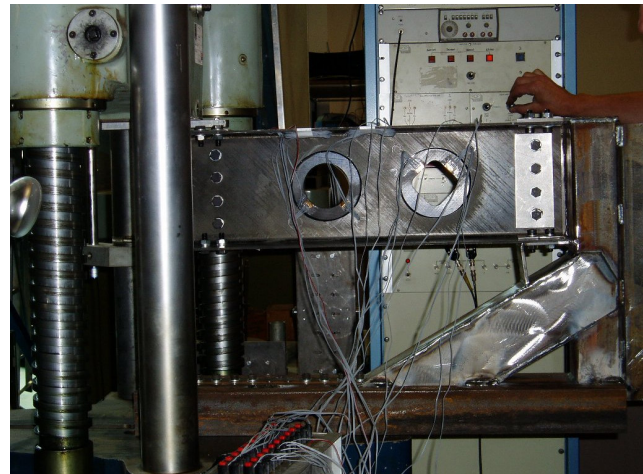


(b)

Figure 5. Maximum principal stress in each ply for Example 2: (a) in the beam web around cutout; (b) in the laminate ring and average stress in steel ring. Note: these stresses were computed at a particular point in the FE model within the strain gauge covered area that is defined as point A.

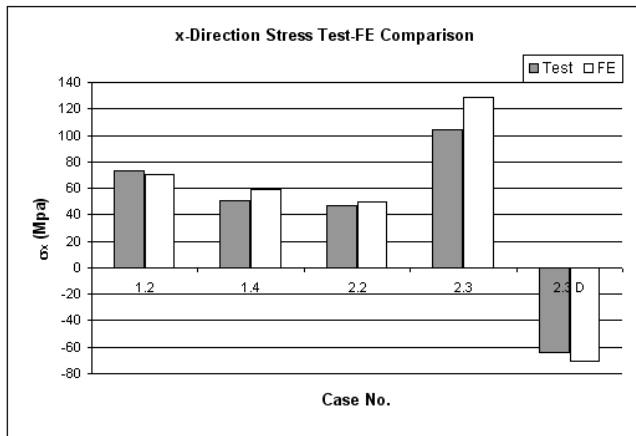


(a)

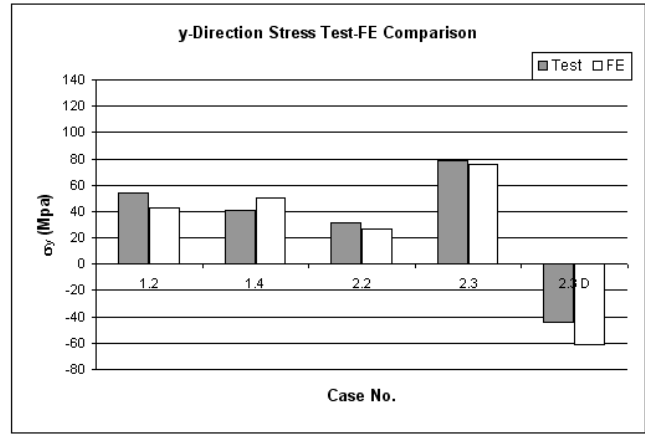


(b)

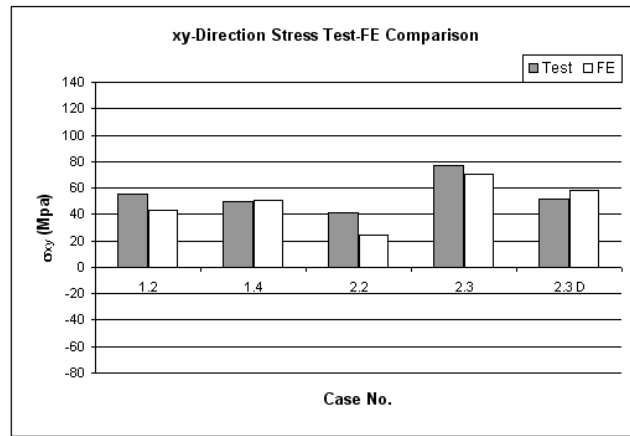
Figure 6. C-section beams mounted on the testing rig: (a) single cutout reinforced by a pair of fibre tow rings; (b) double cutouts reinforced by laminate rings.



(a) *x*-direction



(b) *y*-direction



(c) shear stress on *x*-*y* plane

Figure 7. Comparisons of the test and calculated stresses. Note: numbers on the graph *x*-axis indicate the study case numbers defined in Section 2.3 and Table 2.